Clathrin-dependent entry and vesicle-mediated exocytosis define insulin transcytosis across microvascular endothelial cells

Paymon M. Azizi[a,b,c], Roman E. Zyla[b], Sha Guan[a,b,c], Changsen Wang[b], Jun Liu[c], Steffen-Sebastian Bolz[b], Bryan Heit[d], Amira Klip[a,c], and Warren L. Lee[a,b,c,e]

[a]Institute of Medical Sciences and [e]Interdepartmental Division of Critical Care, Department of Medicine, University of Toronto, Toronto, ON M5S 1A8, Canada; [b]Keenan Research Centre, St. Michael's Hospital, Toronto, ON M5B 1W8, Canada; [c]Programme in Cell Biology, Hospital for Sick Children, Toronto, ON M5G 0A4, Canada; [d]Department of Microbiology and Immunology, University of Western Ontario, London, ON N6A 5C1, Canada

ABSTRACT **Transport of insulin across the microvasculature is necessary to reach its target organs (e.g., adipose and muscle tissues) and is rate limiting in insulin action. Morphological evidence suggests that insulin enters endothelial cells of the microvasculature, and studies with large vessel–derived endothelial cells show insulin uptake; however, little is known about the actual transcytosis of insulin and how this occurs in the relevant microvascular endothelial cells. We report an approach to study insulin transcytosis across individual, primary human adipose microvascular endothelial cells (HAMECs), involving insulin uptake followed by vesicle-mediated exocytosis visualized by total internal reflection fluorescence microscopy. In this setting, fluorophore-conjugated insulin exocytosis depended on its initial binding and uptake, which was saturable and much greater than in muscle cells. Unlike its degradation within muscle cells, insulin was stable within HAMECs and escaped lysosomal colocalization. Insulin transcytosis required dynamin but was unaffected by caveolin-1 knockdown or cholesterol depletion. Instead, insulin transcytosis was significantly inhibited by the clathrin-mediated endocytosis inhibitor Pitstop 2 or siRNA-mediated clathrin depletion. Accordingly, insulin internalized for 1 min in HAMECs colocalized with clathrin far more than with caveolin-1. This study constitutes the first evidence of vesicle-mediated insulin transcytosis and highlights that its initial uptake is clathrin dependent and caveolae independent.**

Monitoring Editor
Keith E. Mostov
University of California, San Francisco

Received: Aug 28, 2014
Revised: Dec 15, 2014
Accepted: Dec 17, 2014

INTRODUCTION

Given the high prevalence of type 2 diabetes, there is an abundance of research into the mechanisms of insulin resistance. Classically, this has focused on impaired insulin signaling in downstream tissues such as muscle and fat. However, this approach carries the underlying assumption that circulating insulin has unimpaired access to its target tissues and can freely bind its receptor on target cells. In fact, after its secretion into the bloodstream by the beta cells of the pancreas, insulin must first cross the endothelial barrier in order to exit the vasculature. Key physiological studies, performed mostly in dogs, show a delay between injected insulin levels and their appearance in interstitial fluids (Yang *et al.*, 1994). Moreover, insulin action in muscle correlates more closely with lymph concentrations of insulin than with those in the circulation (Chiu *et al.*, 2008). Together these observations suggest that transfer across the endothelium is a rate-limiting step in insulin availability.

In theory, the transit of insulin across the endothelial barrier can occur by passive diffusion between cells (paracellular) or by actual transport through individual cells (transcytosis; Armstrong *et al.*, 2012). Insulin's size vis-à-vis the tight nature of the microvascular

This article was published online ahead of print in MBoC in Press (http://www.molbiolcell.org/cgi/doi/10.1091/mbc.E14-08-1307) on December 24, 2014.

Address correspondence to: Warren L. Lee (leew@smh.ca), Amira Klip (amira@sickkids.ca).

Abbreviations used: AF555, Alexa Fluor 555; AF568, Alexa Fluor 568; DN, dominant negative; ELISA, enzyme-linked immunosorbent assay; FITC, fluorescein isothiocyanate; GAPDH, glyceraldehyde 3-phosphate dehydrogenase; HAEC, human aortic endothelial cell; HAMEC, human adipose microvascular endothelial cell; MBCD, methyl-β-cyclodextrin; NA, numerical aperture; NO, nitric oxide; siRNA, small interfering RNA; TEER, transendothelial electrical resistance; TIRF, total internal reflection fluorescence; WT, wild type.

endothelium supplying metabolically relevant tissues such as muscle and fat suggests that transcytosis may be the dominant route for its extravasation (King and Johnson, 1985; Herkner *et al.*, 2003).

Understanding the regulation of insulin transcytosis is important since it may be related to the pathogenesis of insulin resistance (Richey, 2013). Indeed, reductions in nitric oxide (NO) production by the endothelium are characteristic of insulin-resistant states; thus it is intriguing that NO was recently found to stimulate insulin permeability across aortic endothelial cells grown on Transwells (Wang *et al.*, 2013).

Despite its importance, surprisingly little is known of the cell biology of insulin transport across the microvasculature, possibly due to lack of a suitable cellular system. Most of the studies on insulin transcytosis have been performed in endothelia from large vessels (e.g., aorta; Wang *et al.*, 2006, 2013), despite the fact that passage of insulin to tissues in vivo occurs selectively in the *micro*vasculature. This is a critical distinction, since endothelial cells from different tissue beds exhibit numerous important phenotypic and functional characteristics (Aird, 2007a,b). Furthermore, almost all in vitro assays for transcytosis have been performed with cells seeded on Transwells (Boyden chambers). Unfortunately, in this setting, pharmacological or molecular manipulation of endothelial monolayers often induces paracellular gaps (Armstrong *et al.*, 2012), potentially confounding the measurement of actual transcytosis.

Here we report a novel single-cell assay for the quantification of insulin transcytosis across primary adipose microvascular endothelial cells (HAMECs). This approach avoids the potential contribution of paracellular leak and, unlike studies with cell populations, is not affected by poor transfection efficiency, as individual cells can be selected for study. Using this method, we report insulin uptake and its quantal release. In addition, we demonstrate that uptake-limited quantal release requires clathrin- and dynamin- but not caveolin-1–or cholesterol-dependent pathways. In this way, insulin transcytosis differs from the internalization of insulin into aortic cells (Wang *et al.*, 2011) and the transcytosis of proteins such as albumin (Ghitescu *et al.*, 1986).

RESULTS

Insulin is taken up and rapidly secreted by microvascular endothelial cells

We first established that HAMECs in culture express the endothelial cell markers von Willebrand factor and VE-cadherin and exhibit apical/basolateral polarity. HAMEC monolayers display a typical cobblestone morphology and exhibit continuous rings of junctional proteins such as ZO-1 and occludin. Furthermore, as is the case for polarized epithelia (Porter and Hall, 2009; Reglero-Real *et al.*, 2014), HAMECs express ICAM-1 in a polarized manner (Supplemental Figure S1). Thus, morphologically, these cells are a suitable microvascular endothelial model and were used next to study insulin transcytosis.

To begin to analyze the fate of insulin in microvascular endothelial and muscle cells, we delivered a pulse of 500 nM native insulin to monolayers of HAMEC cells (illustrated in Supplemental Figure S1) or L6 myoblasts. After 5 min, the insulin was washed off, and over time, the amount of insulin within cells and that appearing in the supernatant were measured by enzyme-linked immunosorbent assay (ELISA). Under these conditions, HAMECs took up ~10 times more insulin than L6 myoblasts (Figure 1A). Moreover, insulin taken up by myoblasts progressively disappeared, and there was no concomitant, detectable insulin in the overlying media (Figure 1B). In contrast, insulin internalized by HAMECs decreased over time by ~20% in parallel with a progressive recovery of insulin in the supernatant (Figure 1, A and B). To ensure that this behavior of insulin in HAMECs was not the result of saturation of the insulin-processing cellular machinery due to the high levels of insulin used, we repeated these experiments using 50-fold-lower insulin concentration in the pulse, with correspondingly similar results (Supplemental Figure S2).

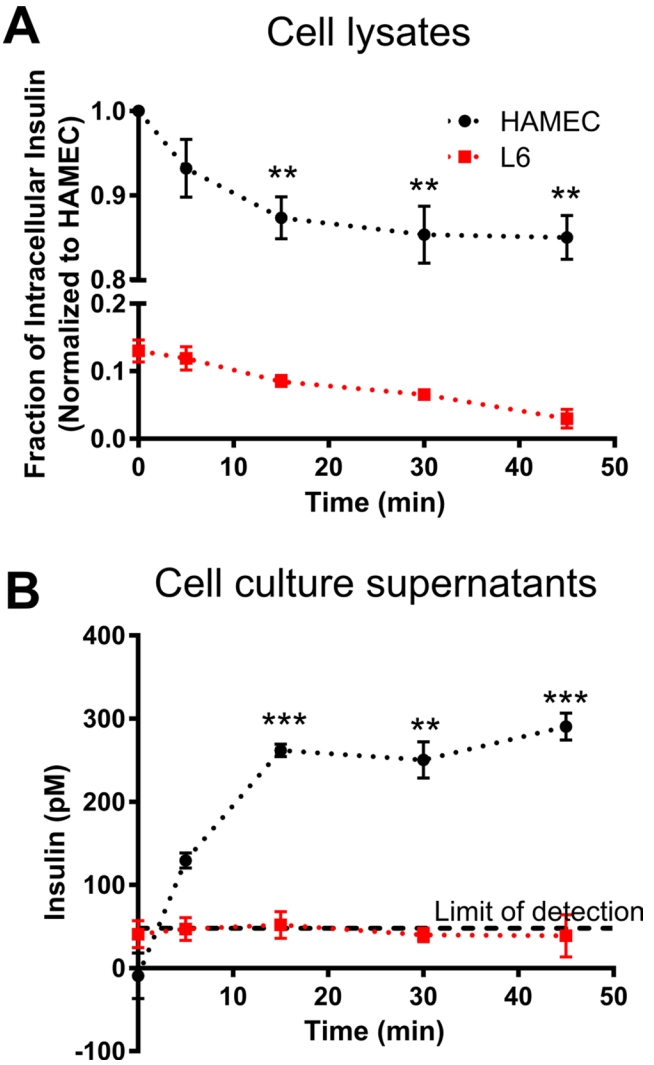

FIGURE 1: Insulin is stored and secreted in HAMECs but degraded in L6 myoblasts. (A) Insulin levels in lysates after a 5-min insulin pulse; data are normalized to initial levels in HAMECs. $^{**}p < 0.01$ compared with initial time point. (B) Insulin levels in cell culture supernatants after a 5-min insulin pulse. $^{**}p < 0.01$, $^{***}p < 0.001$ compared with initial time point.

Insulin is not targeted to lysosomes in microvascular endothelial cells

The permanence of a large fraction of internalized insulin within HAMECs and its contrasting loss within myoblasts is in keeping with the physiological handling of the hormone in the corresponding tissues in vivo. Indeed, circulating insulin should be transported intact across the microvascular endothelium to access its target tissues (e.g., fat, muscle) in order to initiate signaling, where it is eventually degraded through the combined action of insulin-degrading enzyme and muscle/fat lysosomal hydrolysis (Hammons and Jarett, 1980; Duckworth *et al.*, 1998). Accordingly, we examined whether internalized insulin is routed differentially inside microvascular and

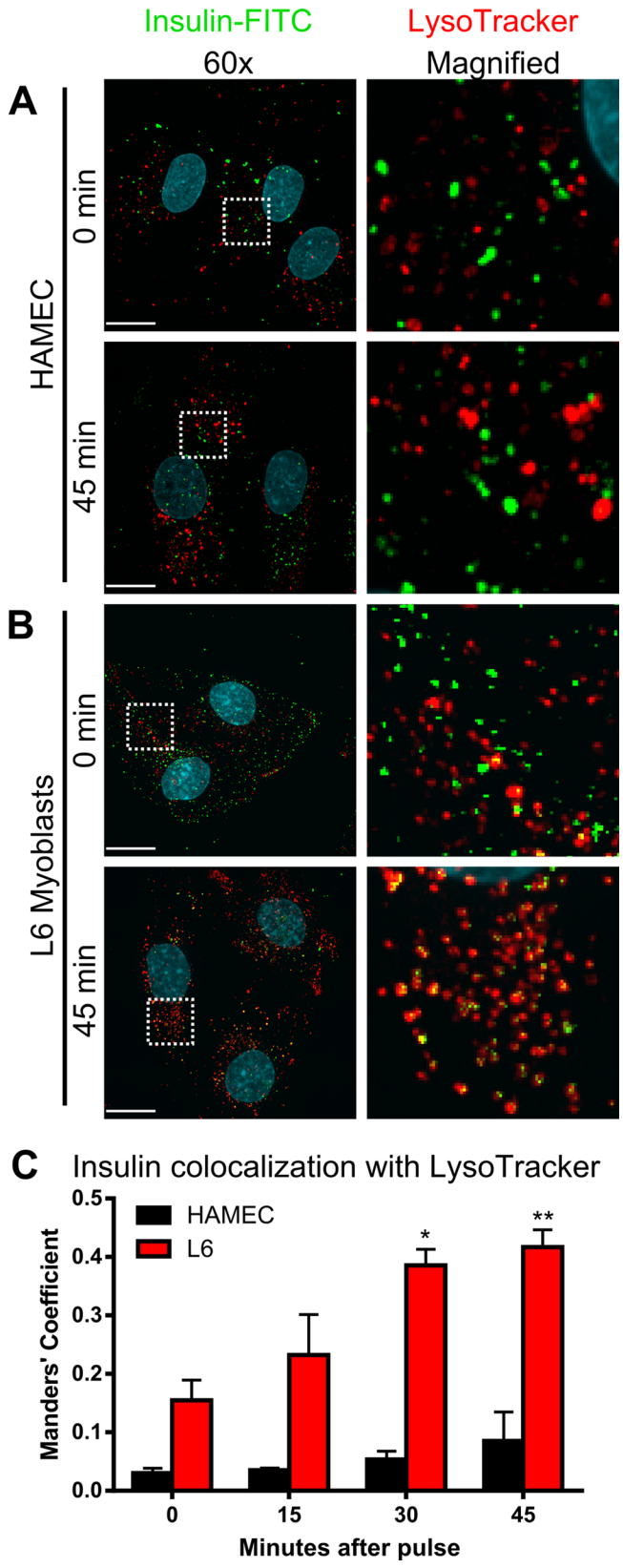

FIGURE 2: Insulin is not targeted to lysosomes in microvascular endothelial cells. (A) Insulin-FITC (green) does not colocalize significantly with LysoTracker (red) at early or late time points. Dashed box indicates area enlarged on the right; white scale, 15 μm. (B) Insulin and LysoTracker colocalization increases over time in L6 myoblasts. Dashed box indicates area enlarged on right; white scale, 15 μm. (C) Quantification of insulin-FITC colocalizing with LysoTracker over time using the Manders coefficient. *$p < 0.05$, **$p < 0.01$ compared with initial time point.

muscle cells. Fluorescein isothiocyanate (FITC)–conjugated insulin (insulin-FITC) internalized by myoblasts accumulated progressively in lysosomes, as shown by the colocalization of the FITC signal with that of LysoTracker, an acidotropic probe that concentrates in lysosomes (Bucci *et al.*, 2000; Figure 2, B and C). In contrast, there was little colocalization of internalized insulin-FITC with lysosomes in HAMECs for the duration of the analysis (Figure 2, A and C). A significant fraction of the insulin-FITC internalized by HAMECs colocalized with transferrin, suggesting their joint retention in early or recycling endosomes (Figure 3). Insulin-FITC retained its bioactivity, as determined by the activation of Akt assayed in muscle cells (Supplemental Figure S3).

Development of an assay to quantify insulin transcytosis by individual endothelial cells

The rapid appearance of insulin in the supernatant of microvascular endothelial cells shown in Figure 1 is consistent with the secretion of internalized insulin (as would be expected for its transcytosis). Mechanistic studies of insulin transcytosis have focused on the endothelium from large vessels, even though these cells are not the physiological route of insulin extravasation, and further have relied on Transwell assays, where insulin delivery from the upper to the lower chamber by transcytosis may be confounded by paracellular leak (Armstrong *et al.*, 2012). To overcome this potential confounder, and, more important, to obtain information on the actual events of insulin secretion at the exit membrane, we used total internal reflection fluorescence (TIRF) microscopy (Figure 4A and Supplemental Movie S1). The assay was combined with the internalization of a pulse of fluorescently conjugated insulin, so that only insulin that binds and is taken up into the cell is then imaged at the ventral membrane. Thus this assay represents a direct assessment of insulin transcytosis. Briefly, a pulse of Alexa Fluor 568 (AF568)–tagged insulin was added to a confluent HAMEC monolayer at 4°C for 10 min, and then insulin-AF568 was washed off and the temperature shifted to 37°C. Immediately thereafter, the ventral membrane was imaged by TIRF microscopy. The live-cell videos were then analyzed in a blinded, automated manner as described in *Materials and Methods* to quantify the number of individual fusion events (vesicle exocytosis) evinced by the abrupt disappearance of individual fluorescent particles (Figure 4B) versus photobleaching of trafficked but nonexocytosed vesicles (Figure 4C).

To ascertain that the criterion of sharp disappearance of individual particles (vesicles) of insulin-AF568 from the TIRF zone is due to insulin exocytosis and not to vesicles trafficking out of the TIRF field, we varied the depth of the TIRF field and recorded the number of insulin-AF568 exocytosis events. Under conditions in which this field is deeper, the probability of vesicle diffusion out of the TIRF field would be expected to diminish, whereas the number of observed exocytic events should remain constant. As hypothesized, the number of detected putative exocytosis events remained the same regardless of the TIRF field depth, confirming that we are detecting exocytic events and not vesicular trafficking out of the TIRF field (Figure 4D).

To validate that the assay measures bona fide transcytosis and is not affected by paracellular leak, we tested the effect of the proinflammatory mediator histamine, a known destabilizer of endothelial barrier integrity (Wu and Baldwin, 1992). Although it rapidly increased endothelial paracellular permeability (Figure 4E),

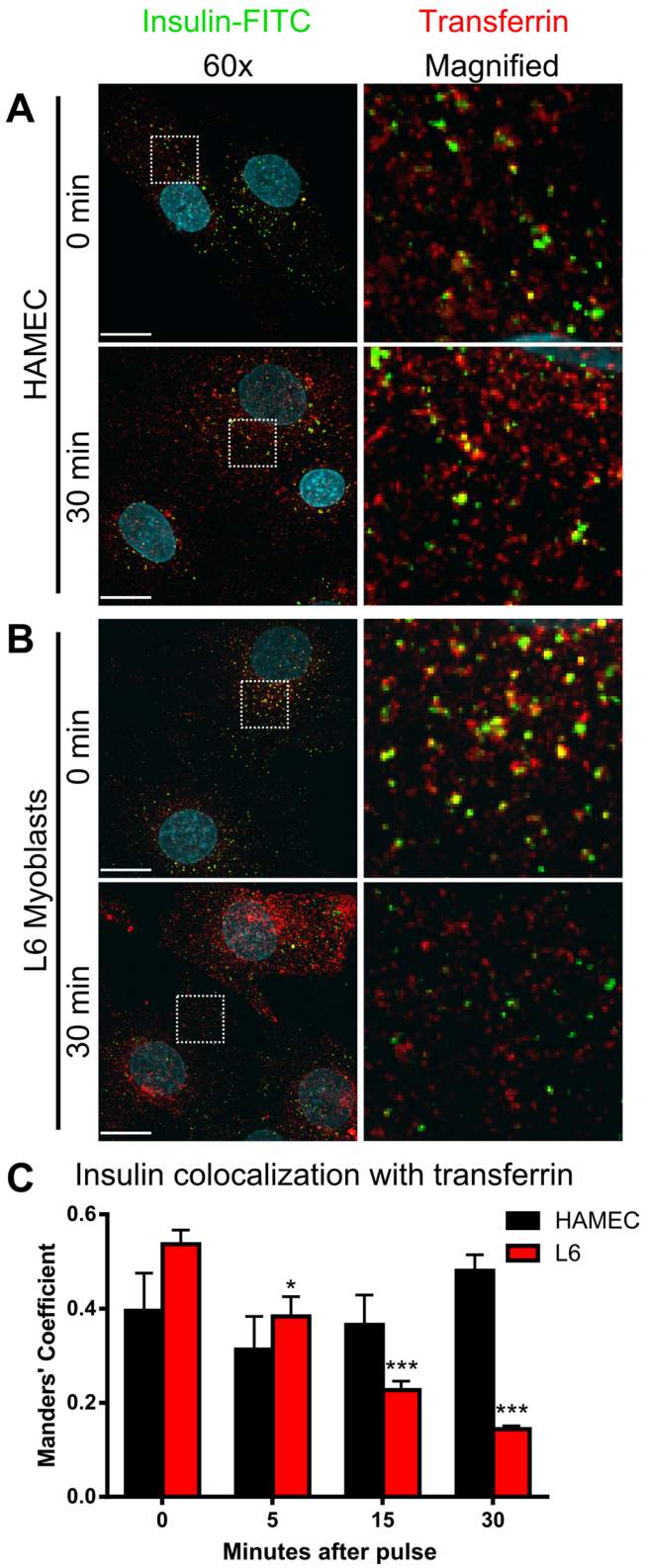

FIGURE 3: Insulin in microvascular endothelium is retained in a transferrin-positive compartment. (A) Insulin-FITC (green) colocalizes moderately with transferrin (red) at early and late time points in HAMECs. Dashed box indicates area enlarged on the right; white scale, 15 μm. (B) Insulin-FITC colocalization with transferrin-AF555 decreases over time in L6 myoblasts. Dashed box indicates area enlarged on the right; white scale, 15 μm. (C) Quantification of insulin colocalizing with transferrin over time using the Manders coefficient. *$p < 0.05$, ***$p < 0.001$ compared with initial time point.

histamine had no effect on the number of detected insulin-AF568 exocytic events (Figure 4F).

To explore whether binding of insulin-AF568 delivered through the pulse involves a saturable step limiting exocytosis, we tested the effect of an excess of unlabeled insulin delivered simultaneously with the fluorescent ligand during the binding at 4°C, followed by insulin-AF568 internalization at 37°C and imaging of exocytic events by TIRF microscopy (Figure 4G). Under these conditions, the TIRF microscopy signal of fluorescent vesicles was essentially abrogated, consistent with competition for a binding site at the uptake step. Hence insulin enters HAMECs through a saturable mechanism rather than by fluid-phase endocytosis or micropinocytosis. To confirm the directional movement of insulin by a second method, we acquired *z*-series images of the intracellular localization of fluorescent insulin taken at 1 and 10 min after insulin binding. Consistent with a transcytotic event, insulin was visible only at or near the apical membrane at 1 min and localized to the bottom of the cell (lower *z*-axis section) by 10 min (Supplemental Figure S4). The latter is consistent with the TIRF results showing that insulin bound at the apical membrane arrives as vesicles at the basolateral surface within 5–15 min.

Having thus validated the assay, we used this approach to establish the time course of insulin transcytosis. After the insulin-AF568 pulse and internalization, the number of insulin exocytic events recorded separately at 1-min intervals increased steadily between 3 and 7 min, after which it progressively declined (Figure 4H). This is consistent with near exhaustion of a releasable pool of insulin-AF568 by 11 min after internalization, a time course consistent with that of the detection of continuous accumulation of preinternalized native insulin in the HAMEC monolayer culture supernatant shown in Figure 1. Finally, to determine whether uptake via fluid-phase endocytosis might have resulted in TIRF-visualized exocytosis, we allowed HAMECs to internalize fluorophore-tagged dextran after a brief pulse (incubation). Under these conditions, HAMECs took up abundant dextran by endocytosis; however, we detected very few dextran exocytosis events by TIRF (Supplemental Figure S5).

Insulin transcytosis is dynamin dependent and does not require cholesterol or caveolin-1

As shown, a saturable step of insulin internalization defines the number of insulin transcytosis events. To analyze further the molecular route of this internalization, we explored the endocytic machineries that may be mediating this mechanism. Treatment of HAMECs with dyngo 4a, a specific inhibitor of the large GTPase dynamin (McCluskey *et al.*, 2013), before and during insulin-AF568 pulsing essentially abrogated its ensuing internalization and transcytosis (Figure 5). Use of dyngo 4a also prevented internalization of Alex Fluor 555–conjugated transferrin (transferrin-AF555, Figure 5A), consistent with the well-known dependence of this phenomenon on dynamin (van Dam and Stoorvogel, 2002).

Dynamin is an essential component of both clathrin-dependent and caveolar-dependent endocytosis. Of interest, Wang *et al.* (2011) observed that insulin uptake into macrovascular endothelial cells from bovine aortae is mediated by caveolae. Caveolae are cholesterol-rich lipid microdomains, and, accordingly, cholesterol depletion or sequestration causes caveolar disassembly. However, depletion of cholesterol using either methyl-β-cyclodextrin (MBCD) or nystatin did not inhibit insulin uptake or transcytosis in HAMECs and instead tended to increase them (Figure 6, A–C). Caveolin-1 is the major protein constituent of caveolae and is required for caveolae generation (Williams and Lisanti, 2004). To our surprise, overexpression of dominant-negative caveolin-1 tended to

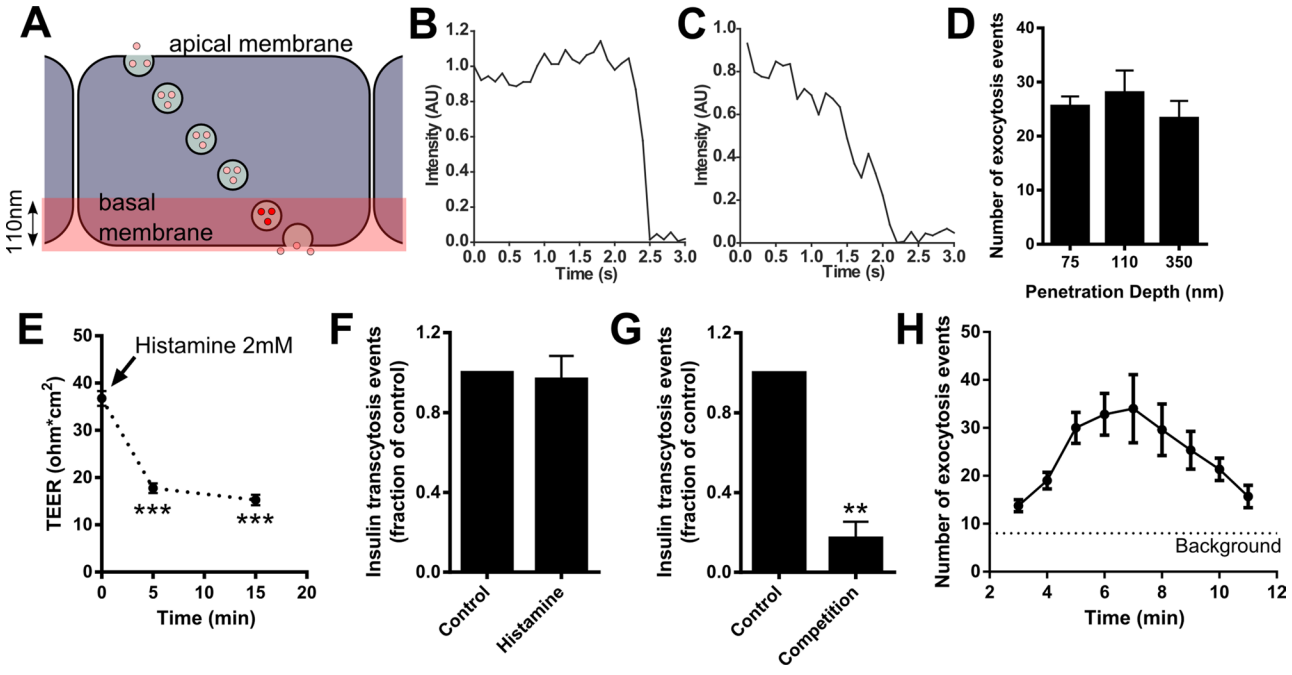

FIGURE 4: Development of a novel single-cell assay to measure insulin transcytosis. (A) Schematic depicting the TIRF microscopy assay. A vesicle bearing fluorescent insulin is visualized as it enters the excitation zone of the endothelial cell and its signal is lost upon fusion with the basal plasmalemma. (B) Intensity profile of a tracked particle that undergoes exocytosis, causing a rapid loss of signal. (C) Intensity profile of a tracked particle undergoing Brownian diffusion (and photobleaching) but not exocytosis. (D) Varying the penetration depth of the TIRF laser does not affect detection events. (E) Transendothelial electrical resistance (TEER) drops after addition of histamine (2 mM) to top and bottom chambers of endothelial cells grown on Transwells (***$p < 0.001$ compared with initial time point) but (F) does not affect the average number of transcytosis events (data are normalized to control cells). (G) Addition of excess unlabeled insulin (50-fold) to the membrane-binding step essentially abrogates insulin-AF568 transcytosis, consistent with a receptor-mediated process. **$p < 0.01$ by one-sample *t* test; data are normalized to control cells. (H) Time course of insulin transcytosis in single cells using the TIRF assay.

promote insulin transcytosis events (Figure 6D), and knockdown of caveolin-1 by small interefering RNA (siRNA) induced a similar trend (Figure 6, E and F). Consistent with these findings, insulin-FITC internalized for 1 min exhibited little colocalization with caveolin-1 in HAMECs (Manders coefficient of 0.196 ± 0.011; Figure 6G). Taken together, these data suggest that insulin transcytosis across adipose microvascular endothelial cells is dynamin dependent but does not occur via caveolae.

Insulin uptake and consequent transcytosis by microvascular endothelial cells requires clathrin

The dependence of insulin uptake and transcytosis on dynamin but not on caveolae suggested an unsuspected role for clathrin in insulin transcytosis. Pitstop 2 is a cell-permeant small molecule that blocks the association of amphiphysin with the terminal domain of clathrin, thereby inhibiting clathrin-mediated endocytosis (von Kleist *et al.*, 2011). We first confirmed that Pitstop 2 effectively blocked the internalization of transferrin, a canonical clathrin-dependent process (Figure 7A). Under these conditions, uptake and transcytosis of fluorescent insulin were reduced by >50% (Figure 7, A–C). Because the specificity of Pitstop 2 has recently been questioned (Dutta *et al.*, 2012), we confirmed our findings by knocking down clathrin heavy chain via cognate siRNA. Depletion of clathrin significantly diminished insulin-AF568 transcytosis (Figure 7, D and E). Consistent with this finding and in contrast to what we observed with caveolin-1, we observed significant colocalization between clathrin and insulin-FITC internalized for 1 min (Manders coefficient is 0.491 ± 0.020; Figure 7F). Hence these results suggest that in HAMECs, insulin internalizes via a clathrin- and dynamin-dependent mechanism, which defines its subsequent availability for quantal exocytosis. In an attempt to reconcile these findings with the caveolar dependence of insulin uptake in bovine aortic endothelial cells (Wang *et al.*, 2011), and cognizant of the heterogeneous nature of endothelial cells, depending on the size and source of their vessels of provenance (Aird, 2007a,b), we explored the possible colocalization of internalized insulin with clathrin or caveolin in human aortic endothelial cells. As anticipated, in these large vessel–derived human endothelial cells, insulin colocalized significantly more with caveolin-1 than with clathrin (Manders coefficient 0.411 ± 0.068 for caveolin-1; 0.196 ± 0.013 for clathrin; Figure 8), paralleling the observations for bovine aortic endothelial cells. These findings underscore the selective insulin uptake processes that take place in endothelial cells of different vascular beds, irrespective of whether they are of bovine or human origin.

DISCUSSION

The endothelium lining every blood vessel differs phenotypically and functionally depending on the size of the blood vessel (e.g., large versus small) and its location in the circulatory system (e.g., arterial versus venous; Ponder and Wilkinson, 1983; Kumar *et al.*, 1987; Craig *et al.*, 1998) Of importance, the passage of nutrients and hormones such as insulin to cells occurs at the level of the *micro*vasculature, as opposed to the primary conduit function served by larger vessels like the aorta (Aird, 2007a,b). Whereas insulin delivery to critical tissues such as muscle and adipose is regulated by vasodilation or constriction that regulates capillary recruitment to

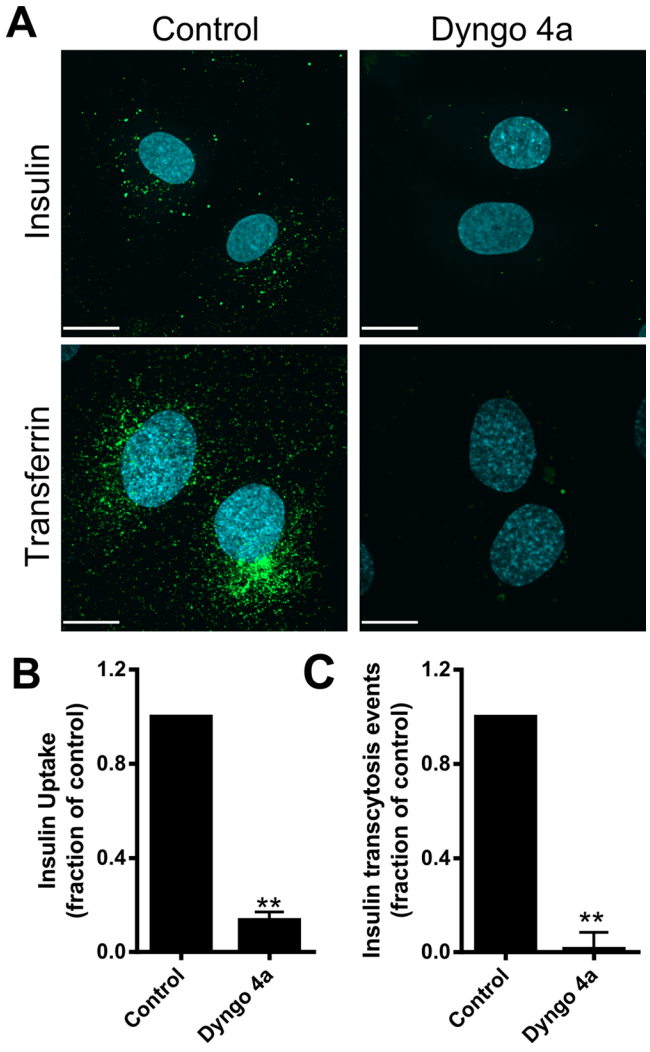

FIGURE 5: Insulin uptake and transcytosis are dynamin dependent. (A) Cells were treated with insulin-FITC or transferrin-AF555 for 10 min after pretreatment with 30 uM dyngo 4a (right) or vehicle (left) for 30 min to impair dynamin function. White scale, 15 µm. (B) Quantification of insulin-FITC uptake in HAMECs after pretreatment with dyngo 4a. $^{**}p < 0.01$ by one sample *t* test; data are normalized to control cells. (C) Average transcytosis events after pretreatment with dyngo 4a. $^{**}p < 0.01$ by one sample *t* test; data are normalized to control cells.

perfuse tissue beds (Bonadonna *et al.*, 1998; Barrett *et al.*, 2011), it is less well appreciated that the transendothelial movement of insulin out of the microvasculature is itself rate limiting for insulin delivery and tissue action (Yang *et al.*, 1994; Majumdar *et al.*, 2012; Kolka and Bergman, 2013). The vasoactive properties governing insulin delivery are relatively well studied; in contrast, surprisingly little is known about the molecular mechanism by which insulin crosses the endothelium and exits the microvasculature. This process is particularly suitable for in vitro studies, since unlike experiments in whole animals, cell culture is not confounded by issues of blood flow and perfusion pressure.

The endothelium of microvessels supplying skeletal muscle and fat is continuous (i.e., without gaps, unlike the hepatic endothelium), and early work indicated that transendothelial insulin permeability in vitro is a saturable, temperature-sensitive, receptor-mediated process (King and Johnson, 1985). In vivo, however, it is debated whether the process of insulin transport across the endothelium is saturable (Eggleston *et al.*, 2007; Majumdar *et al.*, 2012) or not (Steil *et al.*, 1996). The controversy may arise in part due to the influence of various parameters, including hemodynamic ones, on the measurements of transendothelial transport in vivo.

Recently caveolin-1 was shown to be required for endothelial insulin uptake in the aorta and, by implication, for its transcytosis, analogous to its involvement in the transcytosis of albumin in lung endothelial cells (Schubert *et al.*, 2001; Wang *et al.*, 2011). Thus evidence suggests that internalization of insulin by large-vessel endothelia is likely mediated by caveolae. Whether the same is true for the microvascular endothelium, however, is unknown. Moreover, the physiological significance of insulin uptake by endothelial cells of large vessels is unclear, although certainly insulin signaling in those vessels is of critical importance for the regulation of vascular tone.

Current assays for transcytosis have relied on cells seeded on Transwells. Unfortunately, this approach is vulnerable to the induction of discontinuities in the endothelial monolayer causing potential confounding by the resulting paracellular leak. This, combined with the reported poor transfection efficiency of primary endothelial cells, has limited our knowledge of the cellular and molecular regulation of insulin transcytosis. In the present study, we report a novel single-cell assay for insulin transcytosis that obviates these issues. Using primary HAMECs, this method is based on saturable insulin binding and intracellular delivery of the hormone in discrete vesicles that can be imaged at the TIRF zone and undergo exocytosis at the ventral membrane.

Distinctive characteristics of insulin uptake and transcytosis in HAMECs

Insulin uptake by HAMECs is distinct from the uptake of the hormone by muscle cells or endothelial cells of larger vessels. First, insulin uptake in HAMECs is ~10 times higher than that in L6 myoblasts assayed under identical conditions. Second, whereas insulin internalized by myoblasts is routed to lysosomes and is readily degraded, insulin internalized by HAMECs is stable, and a fraction of it undergoes recycling/exocytosis to the medium. This exocytosis is quantal and likely representative of insulin exocytosis at the basolateral side of endothelial cells in vivo. Of course, we cannot say with certainty whether insulin exocytosis at the ventral membrane of HAMECs adhered to a glass coverslip is directly equivalent to its exocytosis toward the interstitial space in vivo.

A large fraction of insulin internalized by HAMECs colocalizes with internalized transferrin, indicating its retention within elements of the endocytic pathway. Future studies should explore the nature of the insulin storage compartment in HAMECs, how it is sorted away from delivery to lysosomes, and whether it can be further induced to undergo exocytosis through selective signals or cell growth conditions. In this regard, it is clearly acknowledged that HAMECs are only a tissue culture model and, although of primary origin, are expected to differ through cellular passages and ex vivo culturing conditions from the endothelial cells constituting the microvessels. Therefore the results obtained with HAMECs are considered a guide for future exploration of the mechanism of insulin transcytosis across the actual microvasculature in vivo. Nonetheless, HAMECs represent a more faithful model of the endothelial cells enacting insulin transcytosis in vivo than do endothelial cells derived from larger vessels. Indeed, our results show that insulin internalization differs in HAMECs and aortic endothelial cells, being mediated by clathrin in the former and possibly by caveolae in the latter; it is also reasonable to speculate that if the *route* of uptake is different between macrovascular and microvascular endothelial cells, other

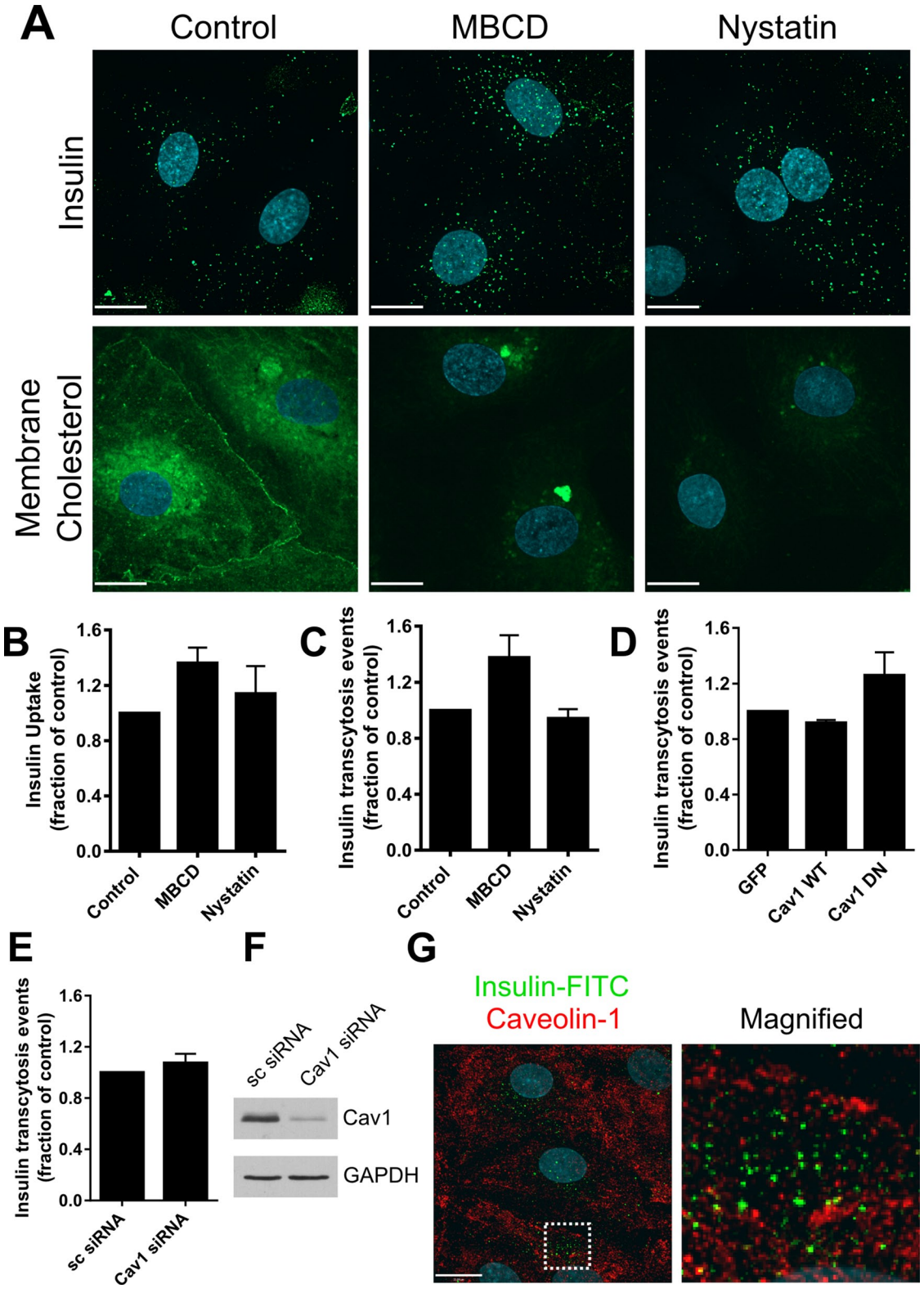

FIGURE 6: Insulin uptake and transcytosis do not require cholesterol or caveolin-1. (A) Cells were treated with insulin-FITC or D4 membrane cholesterol probe for 10 min after pretreatment with either 1 μM methyl-β-cyclodextrin (MBCD) or 50 μg/ml nystatin to deplete cells of cholesterol. White scale, 15 μm. (B) Quantification of insulin-FITC uptake in HAMECs after pretreatment with MBCD or nystatin; data are normalized to control cells. (C) Average transcytosis events after pretreatment with MBCD or nystatin. (D) Average transcytosis events of insulin-AF568 after transfection with wild-type or dominant-negative (DN) caveolin-1 construct. (E) Average transcytosis events of insulin-AF568 after caveolin-1 was knocked down by siRNA. (F) Immunoblot of caveolin-1 protein after knockdown via siRNA. (G) Insulin-FITC colocalizes only modestly with caveolin-1 (red). Colocalization was quantified via the Manders coefficient, which is 0.196 ± 0.011. Dashed box indicates area enlarged on the right; white scale, 15 μm.

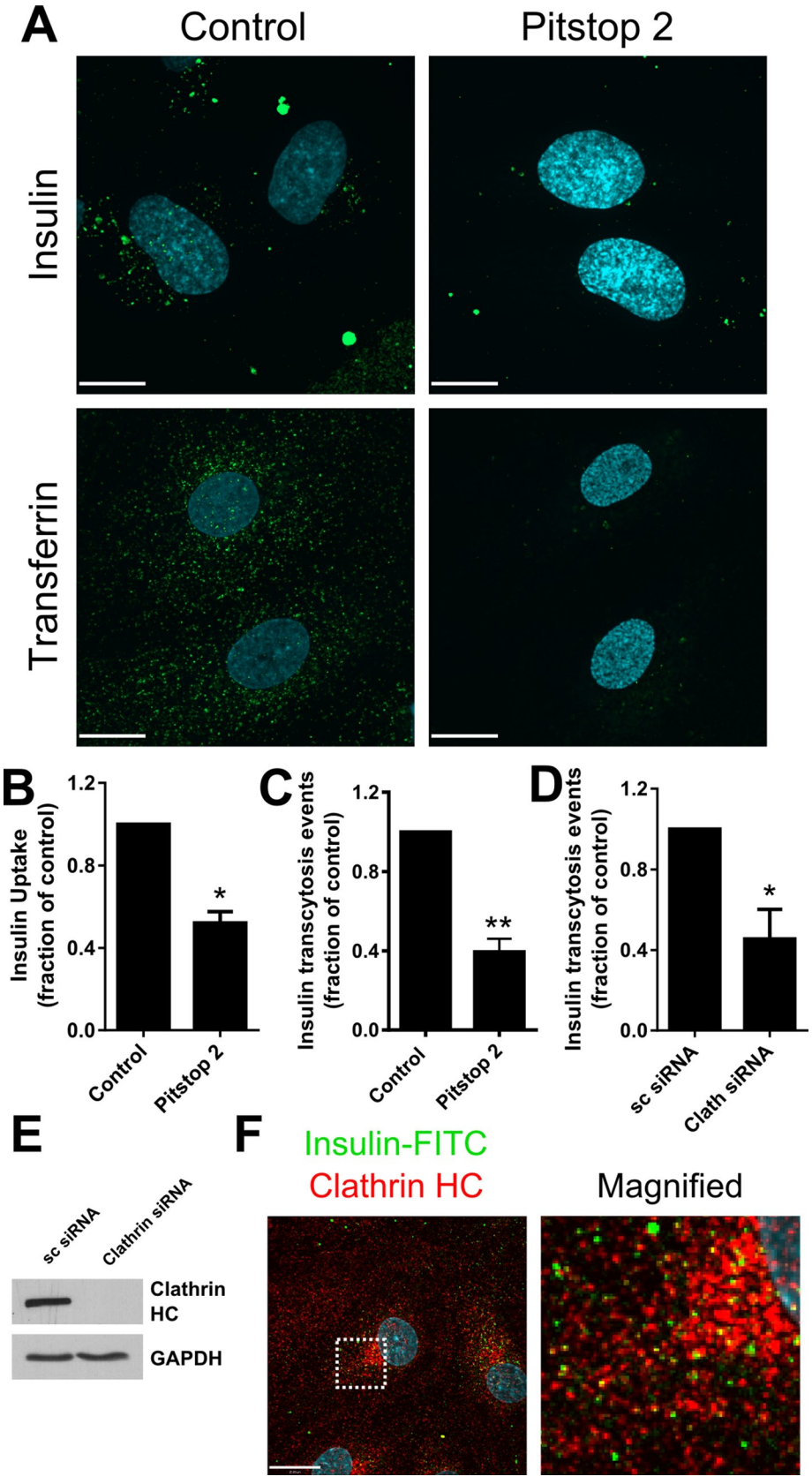

FIGURE 7: Insulin uptake and transcytosis are clathrin dependent. (A) Cells were treated with insulin-FITC or transferrin-AF555 for 10 min after pretreatment with 10 μM Pitstop 2 to impair clathrin-mediated uptake. White scale, 15 μm. (B) Quantification of insulin-FITC uptake in HAMECs after pretreatment with Pitstop 2. (C) Average insulin-AF568 transcytosis events after pretreatment with Pitstop 2. (D) Average insulin-AF568 transcytosis events after clathrin heavy chain was knocked down by siRNA. (E) Immunoblot of clathrin heavy chain protein after knockdown by siRNA. (F) Insulin-FITC (green) colocalizes with clathrin heavy chain (red). Colocalization was quantified via the Manders coefficient, which is 0.491 ± 0.020. Dashed box indicates area enlarged on the right; white scale, 15 μm.

important differences, such as the *rate* of insulin uptake, may also exist. The choice of human adipose tissue as the source of HAMECs was based on the importance of insulin delivery to this tissue, given the prominent role of insulin action in fat cells toward the control of lipolysis and adipokine secretion affecting whole-body metabolism. It is possible that insulin transcytosis in HAMECs is representative of the equivalent phenomenon in endothelial microvascular cells of other metabolically relevant tissues such as muscle, but future studies could also explore potential differences among microvascular cells of different tissue origins.

A further advance represented by the results reported here lies in the recording of actual exocytosis of internalized insulin. To the best of our knowledge, our assay combining saturable insulin binding/internalization and subsequent analysis of its quantal delivery at the ventral membrane constitutes the first in vitro assay of cellular transcytosis of the hormone. Moreover, the system lends itself to molecular interventions that have allowed us to explore the mechanisms involved in insulin uptake.

At a broader level, our novel single-cell assay of transcytosis in HAMECs will greatly facilitate the study of endothelial transcytosis, a fundamental cellular process described decades ago for ligands including albumin, vitamin B12, and immunoglobulins (Tuma and Hubbard, 2003). Using this approach, we are continuing to elucidate the downstream signaling implicated in insulin transcytosis, including an understanding of how insulin evades intracellular degradation. Although the insulin receptor would seem like the prime candidate to mediate transcytosis, a murine endothelial-specific knockout demonstrated little change in glucose homeostasis (Vicent *et al.*, 2003). Thus ongoing work in our labs will determine whether the insulin receptor is required for endothelial transcytosis or whether other receptors fulfill this role. Finally, it is possible that impaired insulin transcytosis contributes to the pathophysiology of insulin resistance or diabetes; elucidating its underlying molecular mechanisms may therefore be important for the identification of targeted therapeutic approaches to improve vascular insulin delivery to tissues.

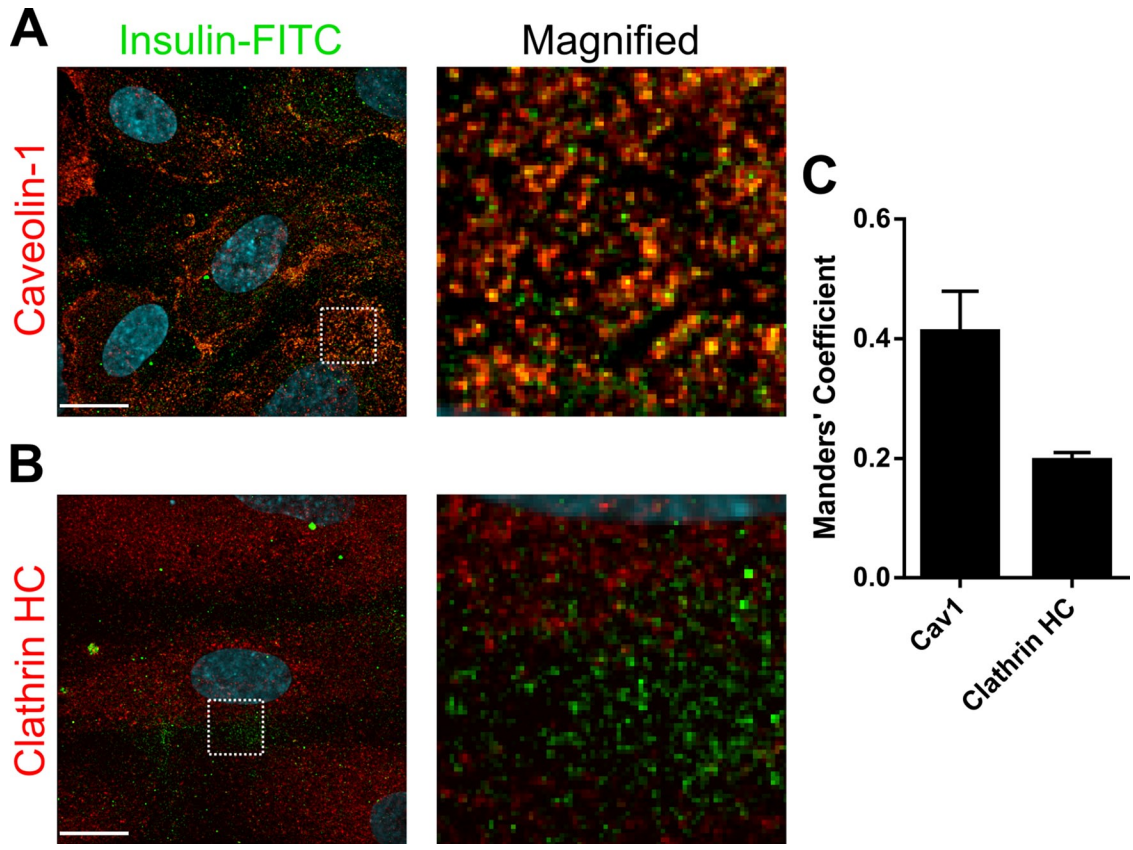

FIGURE 8: Insulin colocalizes with caveolin-1 in HAECs. (A) Insulin-FITC (green) colocalizes with caveolin-1 (red) in HAECs. Dashed box indicates area enlarged on the right; white scale, 15 μm. (B) Insulin-FITC (green) colocalizes with clathrin heavy chain (red) to a much lesser extent than caveolin-1 in HAECs. Dashed box indicates area enlarged on the right; white scale, 15 μm. (C) Quantification of colocalization of insulin-FITC with caveolin-1 (0.411 ± 0.068) or clathrin heavy chain (0.196 ± 0.013) via the Manders coefficient.

MATERIALS AND METHODS

Cell culture

HAMECs were isolated from human visceral fat of nondiabetic patients undergoing abdominal surgery unrelated to this study at St. Michael's Hospital, Toronto. Written informed consent for tissue utilization was obtained, and the study was approved by the institution's Research Ethics Board (REB#11-198). To isolate HAMECs, human visceral adipose tissue fragments were digested using collagenase II, and endothelial cells were sorted out using Dynabeads CD31 (beads loaded with antibody to CD31; Invitrogen, Carlsbad, CA). After isolation, ~95% of these cells expressed von Willebrand factor (vWF) and VE-cadherin and exhibited typical cobblestone morphology under phase contrast microscopy, confirming their endothelial phenotype (Supplemental Figure S1). Cell cultures were expanded and used for experiments between passages 5 and 8. Primary HAMECs were also purchased from ScienCell (Carlsbad, CA); in pilot experiments, no morphological or functional differences could be detected between commercially obtained HAMECs and those isolated in our lab from adipose tissue, and hence they were then used interchangeably throughout this study. Primary human aortic endothelial cells (HAECs) were purchased from Lonza (Allendale, NJ). Endothelial cells were cultured in EGM-MV medium (Lonza, Allendale, NJ) in an incubator at 37°C and 5% CO_2. Cells were always plated on gelatin-coated glass coverslips and used within 48 h of reaching confluence. L6 myoblasts were cultured in α-minimal essential medium supplemented with 10% fetal bovine serum. In some experiments, cells were seeded on gelatin-coated, 12-well Transwell inserts with membrane pore size of 0.4 μm (Costar 3460; Corning, Corning, NY) and grown until confluency as assessed by measurement of the transendothelial electrical resistance using the Endohm-12 (WPI, Sarasota, FL). In other experiments, to induce ICAM-1 expression, HAMECs were exposed to lipopolysaccharide (100 ng/ml; L2880; Sigma-Aldrich, St. Louis, MO) for 18 h.

Electroporation and transfection

HAMECs were electroporated as previously described (Hernandez *et al.*, 2004). Before electroporation, cells were resuspended in Opti-MEM (Life Technologies, Grand Island, NY) with 10% fetal bovine serum at a concentration of 3×10^6 cells/ml. The cell suspension was chilled at 4°C for 10 min before electroporation. To transfect plasmid constructs, cells were electroporated using ECM 830 (BTX, Holliston, MA) at a setting of 200 V for 45 ms. At 18 h after electroporation, medium was changed, and cells were imaged 6–30 h afterward. Cells were transfected with pEGFP-N1 (Clontech, Mountain View, CA), Cav1-GFP (plasmid 14433; Addgene, Cambridge, MA), or Cav1 DN-GFP (plasmid 27708, Addgene).

siRNA was delivered using Lipofectamine RNAiMAX transfection reagent in accordance with the manufacturer's instructions (Life Technologies). Briefly, cells were treated with siRNA 24 h after plating. At 24 h later, a second dose of siRNA was delivered. The cells were used 48 h later; effective knockdown was confirmed by immunoblotting. The following functionally verified siRNAs from Qiagen (Valencia, CA) were used: AllStars Negative Control siRNA (SI03650318), Hs_CAV1_10 FlexiTube siRNA (SI00299642), and Hs_CLTC_10 FlexiTube siRNA (SI00299880).

Confocal fluorescence microscopy

For colocalization experiments, cells were pulsed with 500 nM insulin-FITC (I2383; Sigma-Aldrich) for 5 min at 37°C, and LysoTracker Deep Red (Life Technologies) was added 10 min before fixation; alternatively, cells were incubated with transferrin conjugated to Alexa Fluor 555 (transferrin-AF555; Life Technologies) for the duration of the experiment. For insulin uptake experiments, cells were pretreated with 30 µM dyngo 4a (Abcam, Cambridge, MA), 1 mM methyl-β-cyclodextrin (Sigma-Aldrich), 50 µg/ml nystatin (Bioshop Canada, Burlington, Canada), or 10 uM Pitstop 2 (Abcam). Afterward, cells were treated with 500 nM insulin-FITC for 10 min before fixation. As a control for cholesterol depletion, membrane cholesterol was assessed with a recombinant green fluorescent protein (GFP)–tagged D4 probe kindly provided by Greg Fairn (Keenan Research Centre, St. Michael's Hospital, Toronto, ON, Canada; Shimada *et al.*, 2002). Cells were treated with recombinant GFP-D4 (15 µg/ml) for 10 min before fixation. Cells were fixed with 4% paraformaldehyde for 30–60 min and afterward incubated with 0.15% glycine for 15 min. For immunofluorescence, cells were permeabilized postfixation with 0.1% Triton X-100 for 20 min. The following antibodies were used: anti-caveolin-1 (N-20; Santa Cruz Biotechnology, Santa Cruz, CA), anti-clathrin (ab2731; Abcam), anti-vWF (ab6994; Abcam), anti–VE-cadherin (C-19; Santa Cruz Biotechnology), goat anti-mouse Cy3 (115-166-003; Jackson ImmunoResearch, West Grove, PA), rabbit anti-goat Alexa Fluor 488 (305-546-003; Jackson ImmunoResearch), and donkey anti-rabbit Alexa Fluor 555 (A-31572; Invitrogen). Anti-ICAM1 was from R&D Systems (Minneapolis, MN; BBA4). Primary antibodies were incubated at a dilution of 1:100 for 1 h at room temperature. Secondary antibodies were incubated at 1:1000 for 1 h at room temperature. Coverslips were mounted in fluorescent mounting medium (Dako, Carpinteria, CA) supplemented with 4′,6-diamidino-2-phenylindole (1 µg/ml). Images were acquired with an Olympus IX81 spinning disk confocal microscope with a 60×/1.35 numerical aperture (NA) oil immersion objective with settings kept constant between conditions. Images were deconvolved using Volocity 6.3 (PerkinElmer, Waltham, MA). The fluorescence intensity of images was assessed by ImageJ (National Institutes of Health, Bethesda, MD). Image colocalization analysis was performed using Manders colocalization measurements via JACoP plug-in for ImageJ (Bolte and Cordelieres, 2006).

TIRF microscopy

To visualize insulin arriving at the ventral membrane, we used TIRF microscopy. Because insulin-FITC photobleaches rapidly, we generated insulin-AF568 by conjugating untagged insulin (Sigma-Aldrich) with Alexa Fluor 568–succinimidyl ester as outlined in the Molecular Probes manual (A-20003; Life Technologies). Free, unbound fluorophore was separated using Amicon Ultra 0.5-ml 3k centrifugal filters with multiple washes (Millipore, Bedford, MA). Retention of biological activity of both forms of fluorophore-tagged insulin was verified by immunoblotting for phosphorylated Akt (Ser-473; see Supplemental Figure S3). For transcytosis experiments, cells were pulsed with 500 nM insulin-AF568 at 4°C for 10 min. Unbound insulin was washed off with phosphate-buffered saline (PBS; containing Mg^{2+} and Ca^{2+}) and then imaged on a heated stand (37°C) in RPMI 1640 medium supplemented with 4-(2-hydroxyethyl)-1-piperazineethanesulfonic acid buffer. To determine whether transcytosis of fluid-phase markers also occurs, HAMECs were allowed to internalize 25 µg/ml dextran tetramethylrhodamine (70 kDa; Life Technologies) at 37°C for 5 min, followed by assessment of transcytosis by TIRF microscopy. Uninternalized dextran was removed by rinsing with PBS before imaging.

TIRF microscopy images were acquired on an Olympus cell TIRF Motorized Multicolor TIRF module mounted on an Olympus IX81 microscope (Olympus, Hamburg, Germany). Samples were imaged using a 150×/1.45 NA objective with 561-nm excitation and an 110-nm TIRF field depth using Volocity software for acquisition. Images (150 per cell) were taken at 10 frames/s. Quantification of transcytotic events was performed in a blinded manner using a vesicular detection and tracking algorithm using custom-written MATLAB scripts developed by Bryan Heit. This algorithm first applies a 0.5-pixel Gaussian filter to remove subresolution noise, followed by a local background subtraction with a local area of 324 pixels^2. Putative vesicles are identified by applying a threshold 10% above the mean image intensity. Vesicles thus identified were then separated from other cellular structures by filtering the threshold-fitted image for objects of the expected size (16–81 pixels^2) and circularity (>0.2). The moving vesicles were then tracked using a maximum-probability assessment of how closely potential tracks resemble free and superdiffusive Brownian diffusion (Crocker and Grier, 1995), followed by quantification of the diffusivity (mean-squared displacement) of each vesicle,

$$\mathrm{MSD} = \left(\sum_{k=1}^{N} \left|x_k^2\right|\right)^{\gamma}$$

Although the traffic of intracellular vesicles is actin/microtubule dependent, the plasma membrane fusion requires that this transport cease and the vesicle stably dock with the plasma membrane before releasing their cargo (Becherer *et al.*, 2007). Thus, by excluding diffusive or superdiffusive (vectorial motion), we restrict our analysis to stationary (and therefore potentially docked) vesicles. As such, we limit our analyses to vesicles displaying subdiffusive behavior ($\gamma < 0.8733$), which deviates significantly from free Brownian diffusion ($\gamma = 1$) or superdiffusive/vectorial motion ($\gamma > 1$). Vesicle traces were segmented in order to capture any vesicles that transition from diffusive or superdiffusive motion to subdiffusive motion. Exocytosis events were then identified in this subdiffusive population by identifying vesicles that undergo a decrease in fluorescence intensity at least 2.5 SDs greater over the final two time points compared with the rate of fluorescence decrease over the duration of the vesicle's track.

The TIRF-based transcytosis assay overcomes the limitations of more conventional Transwell and microscopy assays, as it has the capacity to differentiate true transcytotic events from both permeabilization of endothelial junctions and transient interactions of vesicles with the basolateral plasmalemma (Becherer *et al.*, 2007).

Immunoblotting

Lysates were collected in a lysis buffer containing 50 mM Tris, 150 mM NaCl, and 1% Triton X-100 and were run on an SDS–PAGE using 8–12% polyacrylamide gels. Proteins were transferred onto nitrocellulose membranes and blocked for 1 h with milk. The following primary antibodies were used: anti–caveolin-1 (N-20; Santa Cruz Biotechnology), anti–clathrin heavy chain (C-20; Santa Cruz Biotechnology), anti-occludin (F-11; Santa Cruz Biotechnology), anti–ZO-1 (N-19; Santa Cruz Biotechnology), and anti–phospho Akt Ser-473 (9271; Cell Signaling Technology, Beverly, MA). Primary antibodies were incubated overnight at 4°C, and secondary antibodies conjugated with horseradish peroxidase were incubated for 1 h at room temperature. Membranes were visualized using Amersham enhanced chemiluminescence as per the manufacturer's recommended procedure (GE Healthcare, Piscataway, NJ).

ELISA

Cells were pulsed with either 500 nM insulin for 5 min or 10 nM insulin for 10 min at 37°C. Cells were collected in a lysis buffer containing 50 mM Tris, 150 mM NaCl, and 0.25% Triton X-100, sheared using a

27-gauge needle, and freeze thawed once. Protein concentration was assessed using the bicinchoninic acid assay, and equal concentrations were loaded in each well. The ELISA for insulin was performed in accordance with the manufacturer's protocol (RAB0327; Sigma-Aldrich).

Statistical analyses

Unless indicated otherwise, all experiments were performed at least three times. Analyses were performed using Prism software (GraphPad, La Jolla, CA). Multiple comparisons were performed using one-way analysis of variance with Dunnett's post hoc test for comparisons to control. Normalized data were assessed with a one-sample *t* test. Data are presented as mean ± SE.

ACKNOWLEDGMENTS

This work was funded by operating grants from the Canadian Institutes of Health Research (MOP#130493 to A.K. and W.L.L. and MOP-123419 to B.H.) and from the Canadian Diabetes Association (OG-3-12-3838-AK to A.K. and W.L.L.). P.M.A. was supported in part by a graduate award from the Banting and Best Diabetes Centre of the University of Toronto. R.Z. was supported in part by a summer studentship from the Banting and Best Diabetes Centre of the University of Toronto; S.G. was supported in part by a summer studentship from the Keenan Research Centre, St. Michael's Hospital. We thank Philip J. Bilan, Costin Antonescu, and Greg Fairn for valuable comments and reagent facilitation and Susan Armstrong for assistance with some initial experiments.

REFERENCES

Aird WC (2007a). Phenotypic heterogeneity of the endothelium: I. Structure, function, and mechanisms. Circ Res 100, 158–173.

Aird WC (2007b). Phenotypic heterogeneity of the endothelium: II. Representative vascular beds. Circ Res 100, 174–190.

Armstrong SM, Khajoee V, Wang C, Wang T, Tigdi J, Yin J, Kuebler WM, Gillrie M, Davis SP, Ho M, *et al.* (2012). Co-regulation of transcellular and paracellular leak across microvascular endothelium by dynamin and Rac. Am J Pathol 180, 1308–1323.

Barrett EJ, Wang H, Upchurch CT, Liu Z (2011). Insulin regulates its own delivery to skeletal muscle by feed-forward actions on the vasculature. Am J Physiol Endocrinol Metabol 301, E252–E263.

Becherer U, Pasche M, Nofal S, Hof D, Matti U, Rettig J (2007). Quantifying exocytosis by combination of membrane capacitance measurements and total internal reflection fluorescence microscopy in chromaffin cells. PLoS One 2, e505.

Bolte S, Cordelieres FP (2006). A guided tour into subcellular colocalization analysis in light microscopy. J Microsc 224, 213–232.

Bonadonna RC, Saccomani MP, Del Prato S, Bonora E, DeFronzo RA, Cobelli C (1998). Role of tissue-specific blood flow and tissue recruitment in insulin-mediated glucose uptake of human skeletal muscle. Circulation 98, 234–241.

Bucci C, Thomsen P, Nicoziani P, McCarthy J, van Deurs B (2000). Rab7: a key to lysosome biogenesis. Mol Biol Cell 11, 467–480.

Chiu JD, Richey JM, Harrison LN, Zuniga E, Kolka CM, Kirkman E, Ellmerer M, Bergman RN (2008). Direct administration of insulin into skeletal muscle reveals that the transport of insulin across the capillary endothelium limits the time course of insulin to activate glucose disposal. Diabetes 57, 828–835.

Craig LE, Spelman JP, Strandberg JD, Zink MC (1998). Endothelial cells from diverse tissues exhibit differences in growth and morphology. Microvasc Res 55, 65–76.

Crocker JC, Grier DG (1995). Methods of digital video microscopy for colloidal studies. J Colloid Interface Sci 179, 298–310.

Duckworth WC, Bennett RG, Hamel FG (1998). Insulin degradation: progress and potential. Endocr Rev 19, 608–624.

Dutta D, Williamson CD, Cole NB, Donaldson JG (2012). Pitstop 2 is a potent inhibitor of clathrin-independent endocytosis. PLoS One 7, e45799.

Eggleston EM, Jahn LA, Barrett EJ (2007). Hyperinsulinemia rapidly increases human muscle microvascular perfusion but fails to increase muscle insulin clearance: evidence that a saturable process mediates muscle insulin uptake. Diabetes 56, 2958–2963.

Ghitescu L, Fixman A, Simionescu M, Simionescu N (1986). Specific binding sites for albumin restricted to plasmalemmal vesicles of continuous capillary endothelium: receptor-mediated transcytosis. J Cell Biol 102, 1304–1311.

Hammons GT, Jarett L (1980). Lysosomal degradation of receptor-bound 125I-labeled insulin by rat adipocytes: its characterization and dissociation from the short-term biologic effects of insulin. Diabetes 29, 475–486.

Herkner H, Klein N, Joukhadar C, Lackner E, Langenberger H, Frossard M, Bieglmayer C, Wagner O, Roden M, Muller M (2003). Transcapillary insulin transfer in human skeletal muscle. Eur J Clin Invest 33, 141–146.

Hernandez JL, Coll T, Ciudad CJ (2004). A highly efficient electroporation method for the transfection of endothelial cells. Angiogenesis 7, 235–241.

King GL, Johnson SM (1985). Receptor-mediated transport of insulin across endothelial cells. Science 227, 1583–1586.

Kolka CM, Bergman RN (2013). The endothelium in diabetes: its role in insulin access and diabetic complications. Rev Endocr Metab Disord 14, 13–19.

Kumar S, West DC, Ager A (1987). Heterogeneity in endothelial cells from large vessels and microvessels. Differentiation 36, 57–70.

Majumdar S, Genders AJ, Inyard AC, Frison V, Barrett EJ (2012). Insulin entry into muscle involves a saturable process in the vascular endothelium. Diabetologia 55, 450–456.

McCluskey A, Daniel JA, Hadzic G, Chau N, Clayton EL, Mariana A, Whiting A, Gorgani NN, Lloyd J, Quan A, *et al.* (2013). Building a better dynasore: the dyngo compounds potently inhibit dynamin and endocytosis. Traffic 14, 1272–1289.

Ponder BA, Wilkinson MM (1983). Organ-related differences in binding of Dolichos biflorus agglutinin to vascular endothelium. Dev Biol 96, 535–541.

Porter JC, Hall A (2009). Epithelial ICAM-1 and ICAM-2 regulate the egression of human T cells across the bronchial epithelium. FASEB J 23, 492–502.

Reglero-Real N, Alvarez-Varela A, Cernuda-Morollon E, Feito J, Marcos-Ramiro B, Fernandez-Martin L, Gomez-Lechon MJ, Muntane J, Sandoval P, Majano PL, *et al.* (2014). Apicobasal polarity controls lymphocyte adhesion to hepatic epithelial cells. Cell Rep 8, 1879–1893.

Richey JM (2013). The vascular endothelium, a benign restrictive barrier? NO! Role of nitric oxide in regulating insulin action. Diabetes 62, 4006–4008.

Schubert W, Frank PG, Razani B, Park DS, Chow CW, Lisanti MP (2001). Caveolae-deficient endothelial cells show defects in the uptake and transport of albumin in vivo. J Biol Chem 276, 48619–48622.

Shimada Y, Maruya M, Iwashita S, Ohno-Iwashita Y (2002). The C-terminal domain of perfringolysin O is an essential cholesterol-binding unit targeting to cholesterol-rich microdomains. Eur J Biochem 269, 6195–6203.

Steil GM, Ader M, Moore DM, Rebrin K, Bergman RN (1996). Transendothelial insulin transport is not saturable in vivo. No evidence for a receptor-mediated process. J Clin Invest 97, 1497–1503.

Tuma P, Hubbard AL (2003). Transcytosis: crossing cellular barriers. Physiol Rev 83, 871–932.

van Dam EM, Stoorvogel W (2002). Dynamin-dependent transferrin receptor recycling by endosome-derived clathrin-coated vesicles. Mol Biol Cell 13, 169–182.

Vicent D, Ilany J, Kondo T, Naruse K, Fisher SJ, Kisanuki YY, Bursell S, Yanagisawa M, King GL, Kahn CR (2003). The role of endothelial insulin signaling in the regulation of vascular tone and insulin resistance. J Clin Invest 111, 1373–1380.

von Kleist L, Stahlschmidt W, Bulut H, Gromova K, Puchkov D, Robertson MJ, MacGregor KA, Tomilin N, Pechstein A, Chau N, *et al.* (2011). Role of the clathrin terminal domain in regulating coated pit dynamics revealed by small molecule inhibition. Cell 146, 471–484.

Wang H, Liu Z, Li G, Barrett EJ (2006). The vascular endothelial cell mediates insulin transport into skeletal muscle. Am J Physiol Endocrinol Metabol 291, E323–E332.

Wang H, Wang AX, Aylor K, Barrett EJ (2013). Nitric oxide directly promotes vascular endothelial insulin transport. Diabetes 62, 4030–4042.

Wang H, Wang AX, Barrett EJ (2011). Caveolin-1 is required for vascular endothelial insulin uptake. Am J Physiol Endocrinol Metabol 300, E134–E144.

Williams TM, Lisanti MP (2004). The caveolin proteins. Genome Biol 5, 214.

Wu NZ, Baldwin AL (1992). Transient venular permeability increase and endothelial gap formation induced by histamine. Am J Physiol 262, H1238–H1247.

Yang YJ, Hope ID, Ader M, Bergman RN (1994). Importance of transcapillary insulin transport to dynamics of insulin action after intravenous glucose. Am J Physiol 266, E17–E25.